

Water Resources Research®



RESEARCH ARTICLE

10.1029/2023WR036965

ENSO Enhances Seasonal River Discharge Instability and Water Resource Allocation Pressure

Key Points:

- El Niño-Southern Oscillation amplifies Pacific watershed river discharge variability, underscoring climate's pivotal role in water cycles
- Vegetation and precipitation synergistically shape river discharge patterns, reflecting ecological and climatic interplay
- Climate warming scenarios predict heightened river discharge instability, emphasizing the need for adaptive water strategies

Minxiang Zhu^{1,2} , Dan Yu^{1,2}, Yiqi Yu^{1,2}, Yi Zheng^{3,4} , Shaobin Li², Ximing Cai⁵ , and Nengwang Chen^{1,2} 

¹State Key Laboratory of Marine Environment Science, Xiamen University, Xiamen, China, ²Fujian Provincial Key Laboratory for Coastal Ecology and Environmental Studies, College of the Environment and Ecology, Xiamen University, Xiamen, China, ³School of Environmental Science and Engineering, Southern University of Science and Technology, Shenzhen, China, ⁴Shenzhen Municipal Engineering Lab of Environmental IoT Technologies, Southern University of Science and Technology, Shenzhen, China, ⁵Department of Civil and Environmental Engineering, University of Illinois at Urbana-Champaign, Urbana, IL, USA

Supporting Information:

Supporting Information may be found in the online version of this article.

Correspondence to:

N. Chen,
nwchen@xmu.edu.cn

Citation:

Zhu, M., Yu, D., Yu, Y., Zheng, Y., Li, S., Cai, X., & Chen, N. (2025). ENSO enhances seasonal river discharge instability and water resource allocation pressure. *Water Resources Research*, *61*, e2023WR036965. <https://doi.org/10.1029/2023WR036965>

Received 20 DEC 2023

Accepted 14 DEC 2024

Abstract The El Niño-Southern Oscillation (ENSO) significantly disrupts Pacific Ocean watershed hydrology, affecting water supply reliability. However, the specific ways in which ENSO affects seasonal river discharge remain underexplored, presenting a significant gap in our understanding of climate-water interactions. Our study reveals that ENSO exacerbates river discharge variability, evident in the dynamics of maximum rise (Dr) and fall (Df) in standardized discharge, and their duration (M). Notably, ENSO augments Dr but shortens M in major rivers like the Yangtze. Employing a novel metric, the Discharge Instability Index (DII), we find that DII surges by at least 69% in El Niño years, particularly in southwestern North American watersheds. Vegetation and precipitation emerge as pivotal in shaping the discharge response to ENSO. Predictive modeling with DII suggests an escalation in discharge instability under climate warming, with a 0.11%–9.46% increase. This insight calls for water managers to integrate ENSO-induced seasonal variations into strategic planning, blending immediate actions like dam regulation with long-term initiatives such as afforestation, to counteract climate-induced water scarcity.

1. Introduction

Water resources play a critical role in human societies and ecosystems (Vörösmarty et al., 2010). Water resource allocation, dependent on water availability, is vital for balancing supply and demand (Eliasson, 2015; Larsen et al., 2016). Climate change has been linked to an increased frequency of El Niño Southern Oscillation (ENSO) events (Cai et al., 2015, 2017; Singh et al., 2022). ENSO impacts wide regions including North and South America, southern and Eastern Asia, South Africa, Australia, and Europe (Sun et al., 2015). Particularly, East Asia, South Asia, and North America are distributed in the terrestrial monsoon regions of the Northern Hemisphere (NHTMR), which significantly influence global and regional hydrological cycles (Wang et al., 2017). These regions have dense populations relying on rainfed agriculture and potable water. ENSO alters precipitation patterns by affecting atmospheric circulation (Good et al., 2021), leading to spatio-temporal changes in river discharge variability (Shrestha & Kostaschuk, 2005). Extremely uneven distribution of river discharge among dry and wet seasons undoubtedly challenges the allocation of water resources (Liu & Yang, 2012), and even causes intensive socio-economic impacts (e.g., human casualties and economic losses) (McPhaden et al., 2006; Siebert et al., 2001). Understanding the air-land-water interaction during ENSO events is crucial in bridging knowledge gaps related to seasonal river discharge anomaly and supporting adaptive management of watershed water resources in a changing climate.

A number of studies have investigated the impact of ENSO on river discharge. It has been observed that ENSO exerted a significant enhancement on the long-term mean and interannual variability of river discharge (Amarasekera et al., 1997; Siam & Eltahir, 2017). ENSO signals were significantly causal for annual river flow in over 36% of global rivers tested (Su et al., 2018). ENSO is often associated with frequent and severe floods as well as droughts (Emerton et al., 2017; Singh et al., 2022). Specifically, El Niño events have been found to result in an increase in the annual maximum streamflow of the lower Yangtze River (Zhang et al., 2007), leading to a 15% increase in flood frequency (Ma et al., 2018). It is worth noting that the impact of ENSO-induced streamflow varies in terms of timing and intensity across different watersheds. For instance, ENSO influences summer and autumn streamflow in the Yangtze River, while it primarily affects winter and spring streamflow in the Pearl

© 2025. The Author(s).

This is an open access article under the terms of the [Creative Commons Attribution-NonCommercial-NoDerivs License](https://creativecommons.org/licenses/by/4.0/), which permits use and distribution in any medium, provided the original work is properly cited, the use is non-commercial and no modifications or adaptations are made.

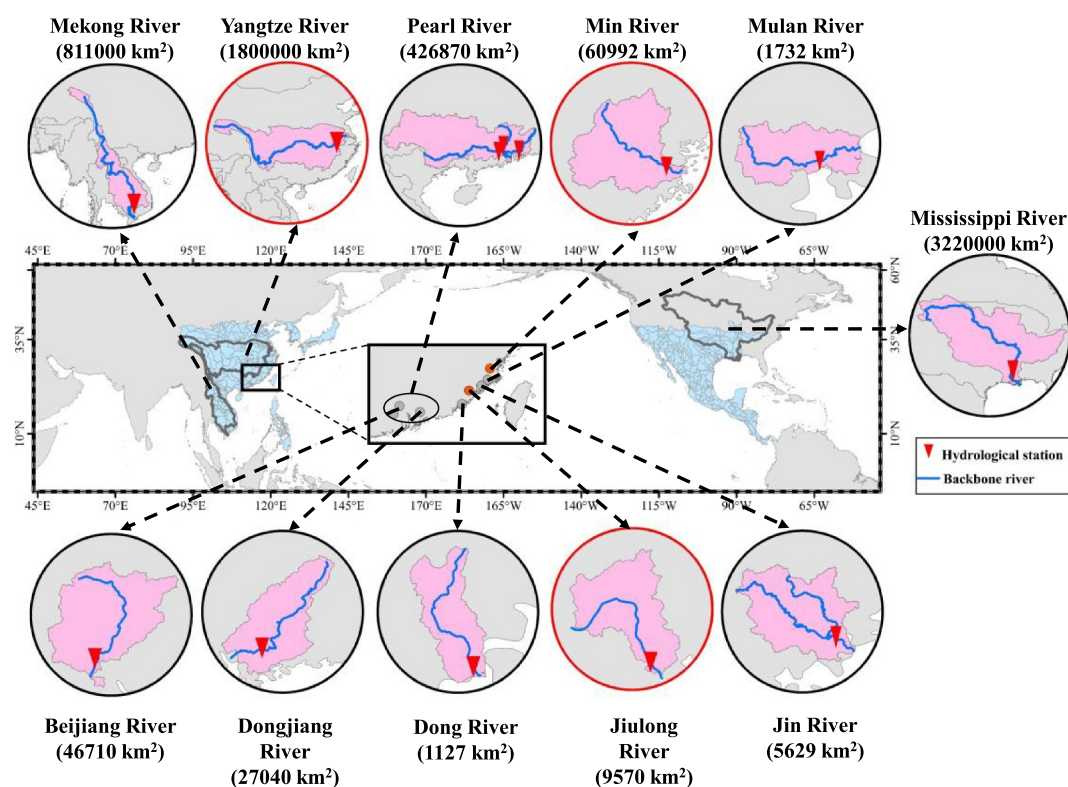


Figure 1. Locations and drainage area of the eleven monitored rivers. Triangles show the hydrological stations in river outlet. The watersheds inside the red circle are the three watersheds for which XGboost is used to simulate natural discharge. The pink watersheds are the watersheds for which monitored discharge is used. The blue watersheds are the 284 watersheds which DII model simulated and predicted in this study.

River. Moreover, the Pearl River experiences larger differences in streamflow (monthly variations exceeding 15%) due to ENSO, compared to the Yangtze River (below 10%) (Ouyang et al., 2014). Recent research has found that watershed characteristics are critical in determining the variability of ENSO-streamflow relationships at the watershed scale, and it has the potential to reveal long-term hydrologic response mechanisms to recurring climate variability (Rice & Emanuel, 2017). Specifically, the normal seasonal distribution pattern of river discharge, indicating the stability of the flow regime (Krasovskaia, 1997), can be disturbed by the ENSO events. However, the research on the underlying mechanisms connecting ENSO events and river discharge instability across different watersheds and regions remains limited.

Our analysis focuses on the regions of South Asia, East Asia, and North America around the Pacific Ocean to investigate the impact of ENSO on seasonal fluctuations in river discharge. ENSO events were grouped based on the Oceanic Niño Index (ONI), which includes strong El Niño, weak El Niño, normal, weak La Niña, and strong La Niña (Table S1 in Supporting Information S1; see Methods for Data collection). First, we observed a significant positive relationship between the river discharge and ONI during strong El Niño years (ONI > 1, shown as El Niño year below) but no clear relationship during other years in three long-term monitored rivers in the period of 1960–2019 (Figure S1 in Supporting Information S1). We then identified the disturbed seasonal distribution patterns via key hydrograph features such as the maximum rise (D_r) and fall (D_f) of monthly standardized discharge and their timespan (M) in eleven monitored watersheds representing South Asia, East Asia, and North America regions (Figure 1). Subsequently, we proposed a new index called discharge instability index (DII) incorporating key hydrograph features (see Methods for Discharge instability index creation) to quantify the uneven seasonal distribution of river discharge during El Niño years compared to normal years. Further, we constructed a DII model (see Methods for DII model construction) incorporating precipitation anomaly and watershed characteristics to explore the current status and the future trend of river discharge instability across 284 watersheds in the study regions. Finally, we discussed regulatory measures aimed at mitigating water resource allocation pressures in watersheds caused by climate change.

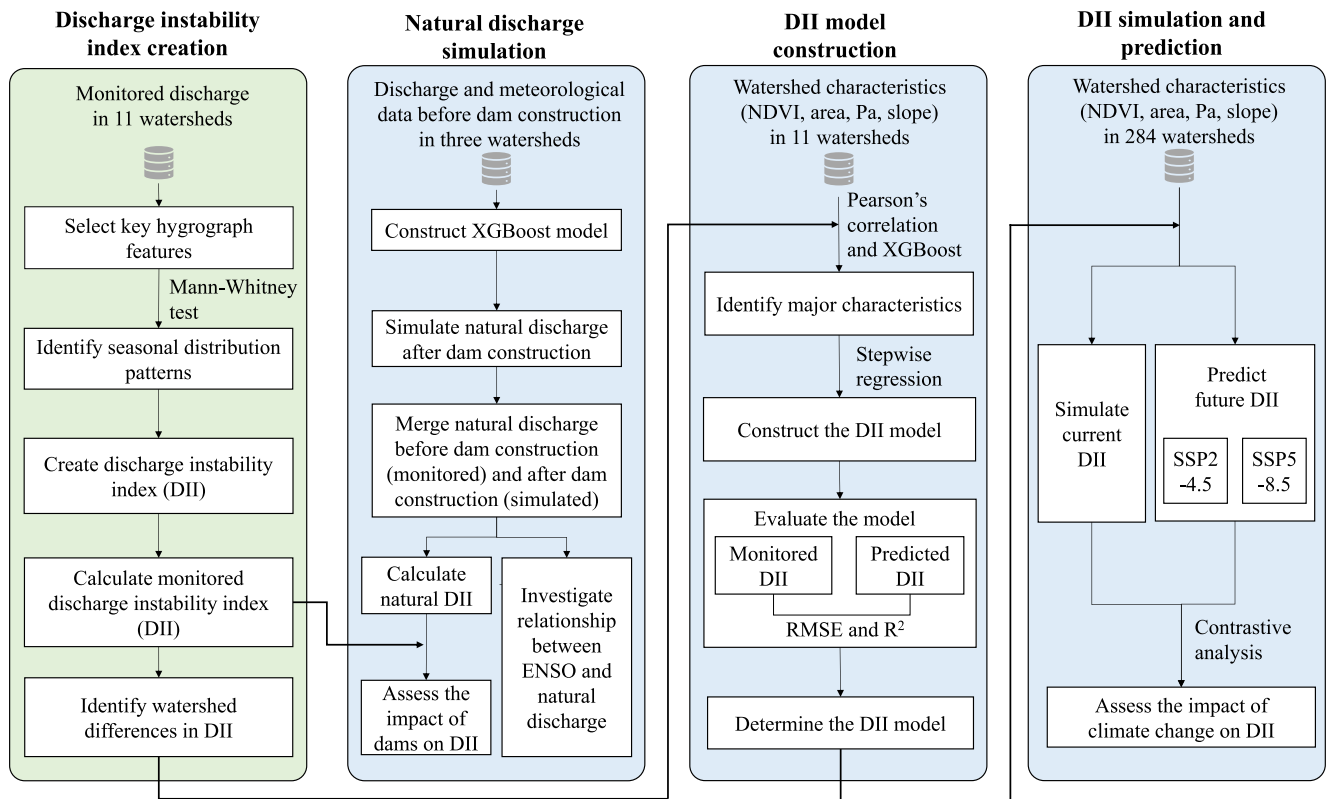


Figure 2. The workflow of the study.

2. Data and Methods

Our study primarily consists of four modules: (a) Creation of discharge instability index (DII) based on monitored flow in eleven rivers: Identifying watershed differences in DII; (b) Simulation of natural discharge by XGboost model for three specific rivers: Investigating the relationship between ENSO and annual natural discharge, and assessing the impact of the dam on DII via natural discharge versus monitored discharge; (c) Construction of a predictive model of DII based on watershed characteristics in eleven rivers; (d) Simulation of current DII, and projection of DII under future warming and precipitation scenarios in 284 watersheds. These components are presented in the workflow diagram (Figure 2) and further explained in the subsequent sections.

2.1. Study Area and Rivers

Our analysis focuses on the regions of South Asia, East Asia, and North America to investigate the impact of ENSO on seasonal fluctuations in river discharge. Eleven monitored rivers located in ENSO-impacted regions were selected for the study (Ward et al., 2014). In order to assess the long-term correlation between ENSO and natural river discharge (see Methods for Natural discharge simulation), we chose three specific rivers: the Jiulong River (represented by its major tributary, the North River), the Min River, and the Yangtze River. These three rivers were selected due to their distinct watershed characteristics and availability of complete long-term hydrometeorological data. Additionally, the monitored discharge data of eleven rivers were used to study seasonal river discharge fluctuations pattern (e.g., Jiulong River, Min River, Yangtze River, Jin River, Mulan River, Dong River, Dongjiang River, Beiji River, and Pearl River in East Asia, Mekong River in South Asia, and Mississippi River in North America). These eleven rivers representing South Asia, East Asia, and North America regions are different in size, climate, and geographic conditions (Figure 1). To explore the region distribution of river discharge instability (DII, see Methods for Discharge instability index), the DII model (see Methods for DII model construction) was applied to 284 watersheds located in the study regions. These watersheds were the individual watersheds of at least 10,000 km² collected from HydroBASINS data, which breakdown sub-basin based on river branch meetings (Lehner & Grill, 2013).

2.2. Data Collection

The Niño Index (ONI) data was collected from Golden Gate Weather Services (<https://ggweather.com/enso/oni.htm>), a resource that has become the de-facto standard that NOAA uses for classifying El Niño (warm) and La Niña (cool) events. It is the running 3-month mean sea surface temperature (SST) anomaly for the Niño 3.4 region (i.e., 5°N–5°S, 120°–170°W). El Niño events are defined as 5 consecutive overlapping 3-month periods with an SST anomaly of +0.5 or higher, while La Niña events are defined as periods with an SST anomaly of –0.5 or lower. In this study, El Niño year was grouped into weak El Niño year ($0.5 \leq \text{ONI} < 1$) and strong El Niño year ($1 \leq \text{ONI}$), likewise, La Niña year was recorded as weak La Niña year ($-1 \leq \text{ONI} < -0.51$) and strong La Niña year ($\text{ONI} \leq -1$); others were grouped as normal years ($-0.5 \leq \text{ONI} \leq 0.5$) (Table S1 in Supporting Information S1).

The national station near the outlet of the watershed is used as the discharge data of the entire watershed. Daily discharge data from 1960 to 2019 were collected from the Punan station on the Jiulong River, the Zhuqi station on the Min River, and monthly discharge data from Datong station on the Yangtze River. Monthly discharge data from other stations (i.e., Shijiao, Boluo, and Gaoyao on Pearl River, Laixi on Mulan River, Zhao'an on Dong River, Shilong on Jin River, Kratie on Mekong River, and Vicksburg on Mississippi River) were obtained from the Global Runoff Data Centre (<https://www.bafg.de>) and Fujian Water Resources Survey Center. These stations are national stations whose locations were carefully determined to ensure representativeness, and the quality of data collected at these stations is high. Additionally, daily meteorological (including precipitation, temperature, wind speed, relative humidity, and solar duration) during the same period were obtained from various weather stations in the watersheds (China Meteorological Data Service Centre, <https://www.cma.gov.cn/> and Climatic Research Unit gridded Time Series V4 (<https://crudata.uea.ac.uk/cru/data/hrgr/>). Watershed vegetation indices (Normalized Difference Vegetation Index) and topographic indices (slope) were collected to investigate the impact of watershed characteristics on DII variations. The GIMMS 3g Normalized Difference Vegetation Index (NDVI) with a spatial resolution of 0.0833° from ECOCAST (<http://ecocast.arc.nasa.gov>) and Digital Elevation Model (DEM) on a 30 by 30 m grid was obtained from the geospatial data cloud platform (<https://www.gscloud.cn/>) for calculating watershed slope. The MODIS NDVI (<https://modis.gsfc.nasa.gov/data>) and the precipitation of DWD's GPCP (https://opendata.dwd.de/climate_environment/GPCP/) were collected to explore bias and potential impacts on results in the uncertainty and limitation section.

2.3. Natural Discharge Simulation

To examine the long-term correlation between ENSO and natural river discharge, which refers to the discharge unaffected by damming, we simulated the natural discharge during periods significantly impacted by dams in three specific rivers (the Jiulong River, the Min River and the Yangtze River) using the XGBoost model (Wang et al., 2023). XGBoost is an ensemble learning algorithm based on decision trees, which can better capture nonlinear relationships in data. The long-term monthly flow data (60a) from those three watersheds supported the application of XGBoost model (see Text S1 in Supporting Information S1 for details of XGBoost model construction process). However, due to incomplete meteorological data, we were unable to simulate the natural discharge for the remaining eight monitored watersheds.

The initiation years of extensive dam constructions in the Jiulong River, Min River, and Yangtze River were 1980, 1982, and 2003, respectively (Zhang et al., 2020). For building the monthly natural discharge model for the Jiulong River, Min River, and Yangtze River, the watershed-wide monthly mean meteorological value (e.g., precipitation, temperature, relative humidity, and wind speed) during 1960–1975, 1960–1975, and 1960–1992 data were used for training, while the data during 1976–1979, 1976–1981, and 1993–2002 were used for validation (Figure S2 in Supporting Information S1) and the data during 1980–2019, 1982–2019, and 2003–2019 were used for testing. The Nash–Sutcliffe model efficiency coefficient (NSE) during the validation period yielded values of 0.73, 0.74, and 0.55, and the square of the Pearson correlation coefficient (R^2) of 0.75, 0.77, and 0.68 for the Jiulong River, Min River, and Yangtze River, indicating acceptable simulation results.

The simulated natural discharge was used for statistical analysis to investigate the correlation between ONI and annual river discharge in the three watersheds. Moreover, in order to investigate the impact of dams on seasonal discharge instability, we compared the difference between natural discharge instability (calculated from simulated natural discharge) and dam regulated discharge instability (calculated from monitored discharge) in the three watersheds.

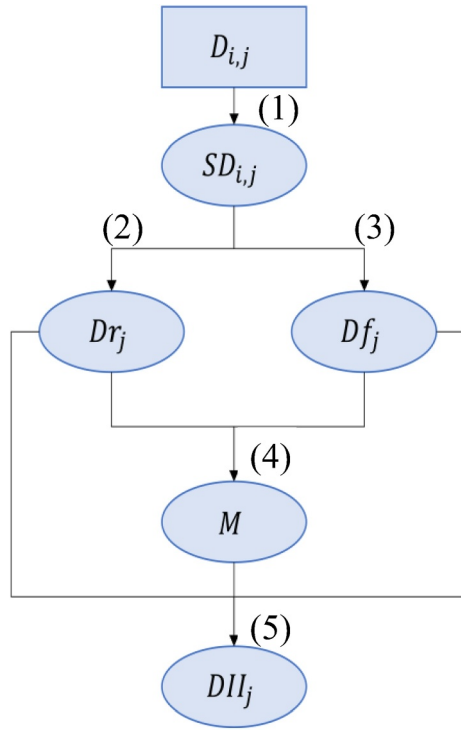


Figure 3. The calculation process of discharge instability index.

2.4. Discharge Instability Index Creation

A new index called discharge instability index (DII) was proposed to assess the uneven seasonal distribution of river discharge during El Niño years compared with normal years, which was proposed by Equations 1–5 and Figure 3.

$$SD_{i,j} = \frac{(D_{i,j} - \bar{D})}{\sigma} \quad (1)$$

$$Dr_j = \max(SD_{i+1,j} - SD_{i,j}) \quad (2)$$

$$Df_j = \min(SD_{i+1,j} - SD_{i,j}) \quad (3)$$

$$M_j = i_{Dfj} - i_{Drj} \quad (4)$$

$$DII_j = (Dr_j/Df_j) \times (Dr_j + Df_j) \times \frac{1}{M_j} \quad (5)$$

where i, j is the i th month of j th year; D is the monitored monthly discharge and \bar{D} is multi-year mean of monitored monthly discharge; σ is the standard deviation; SD is the monthly standardized discharge; Dr_j is the maximum rise of monthly SD between two adjacent months in j th year; Df_j is the maximum fall of monthly SD between two adjacent months in j th year; i_{Dfj} is the i th month which Df appeared in the j th year; i_{Drj} is the i th month which Dr appeared in the j th year; M_j is the timespan of months with the maximum rise

(Dr_j) and the maximum fall (Df_j) in j th year. (Dr_j/Df_j) is the discharge fluctuation deviation term, which reflects the symmetry of the discharge fluctuations. ($Dr_j + Df_j$) is the magnitude of discharge fluctuations, and $\frac{1}{M_j}$ reflects the speed of changes in the discharge fluctuation. The three terms with different units and magnitudes are normalized using the maximum and minimum methods, resulting in values ranging from 1 to 5. This normalization allows for the multiplication of the three terms while maintaining isotropy.

To identify the disturbed seasonal distribution pattern, Mann-Whitney Test was used to assess the significant level of difference in Dr , Df , M , and DII between El Niño years and normal years in eleven monitored rivers. Here, Dr , Df , M , and DII were calculated from the monitored discharge in eleven watersheds.

2.5. DII Model Construction

To explore the current status and the future trend of river discharge instability in study regions, a DII model based on watershed characteristics was constructed. The monitored discharge data and watershed characteristics in eleven watersheds were used for the DII model development. The variables having significant correlation with monitored DII using Pearson's correlation analysis were selected as target variables for the DII model construction. The significance level ($p < 0.05$) was used to identify major watershed characteristics in DII variations across eleven monitored watersheds during El Niño and normal years. Watershed characteristics including annual mean NDVI, watershed mean slope, annual mean Precipitation anomaly (Pa), drainage area (Area), annual mean temperature (Ta), annual mean relative humidity (RH), annual mean wind speed (WS), and annual sunshine duration (SD), which represent the watershed climate, vegetation coverage, and topography. Watershed mean NDVI, Ta, Pa, WS, and SD were counted in El Niño years and normal years. Pa was calculated by Equation 6.

$$Pa = \frac{Pre - \overline{Pre}}{\overline{Pre}} \times 100\% \quad (6)$$

where Pre is the mean of precipitation in the El Niño and normal years; \overline{Pre} is the multi-year mean precipitation. NDVI, Pa (%), slope ($^\circ$), and drainage area (10^4 km^2), which showed a significant correlation with monitored DII variations in eleven watersheds (Figure S3 in Supporting Information S1), were finally selected as the major

watershed characteristics for DII model development. Additionally, the XGBoost model was utilized to ascertain the feature importance of major watershed characteristics in the DII variation. The 100 sets of different random seeds were used to construct the XGBoost model to compute the relative feature importance, and the average was finally taken.

DII model (Linear regression equations) was developed using stepwise regression. The stepwise regression model, which imposes lower demands on the data set, can reduce multicollinearity issues to maintain the stability and reliability of the model. This model incorporates major watershed characteristics (NDVI, Pa (%), slope (°), and drainage area (10^4 km²)) across eleven monitored rivers in the El Niño and normal years, respectively. To validate the regression equations, we utilized a leave-one-out cross-validation approach, with ten out of the eleven monitored watersheds forming the training set and the remaining one serving as the testing set. The Root Mean Squared Error (RMSE) and the square of the Pearson correlation coefficient (R^2) were used to evaluate the model performance. The best-fit model was determined by selecting the equation that showed the smallest RMSE and largest R^2 between the monitored and predicted values. Among the derived regression equations (Figure S4a in Supporting Information S1), the linear regression model for El Niño years (DII_E) was determined as Equation 7 with the smallest RMSE and the largest R^2 . Similarly, the best-fit linear regression model for normal years (DII_N) was determined as Equation 8 (Figure S4b in Supporting Information S1).

$$DII_E = 65.21 - 88.85NDVI + 1.55Pa + 0.32slope - 0.02Area \quad (7)$$

$$DII_N = 24.28 - 30.54NDVI - 0.12Pa + 0.10slope - 0.01Area \quad (8)$$

Considering the significant variations in hydrologic and geographic attributes between the modeled watersheds and other western US watersheds, the DII models (DII_E and DII_N) were also validated in western North America watersheds. The comparison of monitored DII (DII_E and DII_N) and predicted DII (DII_E and DII_N) was conducted in five watersheds with a drainage area of 53,410–634,520 km² (Sacramento River, San Joaquin River, Rio Bravo River, Rio Panuco River, and Colorado River) (Figure S5c in Supporting Information S1). The Root Mean Squared Error (RMSE) and Mean Absolute Percentage Error (MAPE) of DII_E and DII_N models were 1.50% and 6.35%, 0.57% and 8.64%, respectively (Figures S5a and S5b in Supporting Information S1). These validation results have substantiated that our DII model was capable to be applied in broader watersheds not restricted in the selected eleven watersheds.

2.6. DII Simulation and Prediction

The DII models (DII_E and DII_N) were used to simulate watershed mean DII for 284 watersheds in El Niño and normal years respectively. The selected 284 watersheds are geographically close to the eleven monitored watersheds and are similar in climate and drainage area (>10,000 km²). In addition, these watersheds are located between 0 and 40°N around the Pacific Ocean, which is the ENSO-impacted region.

To predict the future trend of DII across the 284 watersheds in response to future climate warming, the DII model of El Niño year (DII_E) was performed with two scenarios: SSP2-4.5 (moderate warming) and SSP5-8.5 (intense warming). SSP2-4.5 and SSP5-8.5 comprise representative concentration pathways and shared socio-economic pathways (Text S2 in Supporting Information S1). The scenario assumes that the future NDVI and Pa are changed, and the slope and drainage area remain unchanged in 284 watersheds. The NDVI in the two scenarios were the current NDVI in El Niño years with a decrease of 0.04% and 0.29%, respectively (Lian et al., 2023). The future precipitation anomaly (Pa) in the two scenarios was the current Pa of the El Niño year with an increase of 15% (Power & Delage, 2018). The predicted DII variation (δ DII) was indicated by relative deviation (%) of future warming scenarios from current El Niño years to explore the future trend of river discharge instability in 284 watersheds.

2.7. Uncertainty Analysis

The DII model incorporates major watershed characteristics (NDVI, Precipitation anomaly (Pa, %), slope (°), and drainage area (10^4 km²)). Comparisons with other data sets were used to explore potential uncertainty in data sources (i.e., NDVI and Pa) and their impact on the findings. Slope and watershed area were not compared with different data sets because they are fixed values for the watershed. The precipitation data in DWD's GPCC based on high observation count was selected for comparison (Harris et al., 2020), which shows high-frequency

agreement with CRU TS v4 used in this study (Becker et al., 2013). For NDVI, the MODIS NDVI was chosen for its high fidelity as comparison to the GIMMS3g NDVI used in this study (Kawamura et al., 2005). Compared to MODIS NDVI, the GIMMS3g NDVI had higher annual mean values (3% higher) (Zhang et al., 2017). However, MODIS NDVI data products have only been available since 2000, which cannot support the construction of DII models. Therefore, we use GIMMS3g NDVI with a 3% decrease to represent MODIS NDVI in this study. The DII models were reconstructed using GPCC and MODIS NDVI, respectively. The comparisons of simulated and predicted DII variations using different data sets in 284 watersheds were used to explore the impact of bias in data sources on results.

The 95% confidence interval estimated via SPSS software (SPSS Statistics 19) was used to explore the potential uncertainty in the stepwise regression method and their impact on the findings.

3. Results

3.1. Seasonal River Discharge Instability

The DII values during El Niño years were significantly higher than during normal years across eleven monitored watersheds ($p < 0.05$, Figure 4a). Meanwhile, the D_r exhibited a similar trend, except for the Mekong River (Figure 4b). The M of the Yangtze River, Mississippi River, and Mekong River were significantly shorter during El Niño years compared to normal years ($p < 0.05$, Figure 4c). No significant difference in D_f between El Niño and normal years was found across eleven watersheds (Table S2 in Supporting Information S1). Based on the variations of D_r and M from normal years to El Niño years, these watersheds were classified into three patterns: DII-I (increased D_r , including Jin River, Mulan River, Jiulong River, Dong River, Min River, Beiji River, Dongjiang River, and Pearl River), DII-II (increased D_r and decreased M , including Mississippi River, Yangtze River), and DII-III (decreased M , including Mekong River) (Table S2 in Supporting Information S1, Figures 4d–4f).

3.2. The Relationship Between DII and Watershed Characteristics

The link between monitored DII and watershed characteristics was used to identify the major watershed characteristics in DII variations in eleven watersheds. The mean monitored DII during El Niño years showed a positive correlation with watershed slope and precipitation anomaly (P_a) in the eleven monitored watersheds. On the other hand, it exhibited a negative correlation with NDVI and drainage area (Figure S3 in Supporting Information S1). Specifically, lower NDVI indicates reduced water retention capacity, while smaller drainage areas result in shorter water residence time within a watershed (Chen et al., 2021), contributing to higher DII values. The XGBoost model showed that NDVI, precipitation anomaly and slope accounted for 48%, 40%, and 10% of the feature importance respectively in explaining the variability of DII among eleven rivers. Drainage area had a significantly lower impact at 2% (Figure 5a).

Comparing the dam-regulated DII (calculated from long-term monitored discharge) with the natural DII (calculated from natural discharge simulated by XGBoost, see Methods for Nature discharge simulation) to explore the impact of dam on DII in three specific rivers. We observed a decrease of 4%–9% in the three watersheds with complete long-term hydrometeorological data during El Niño years (Figure 5b). Notably, the impact of dam regulation on reducing DII was more significant in large river (i.e., Yangtze River) than in small rivers (i.e., Jiulong River and Min River).

3.3. The Modeled Discharge Instability Index

We applied DII_E (Equation 7) and DII_N (Equation 8) to the 284 watersheds (drainage area $> 10,000 \text{ km}^2$) in the tropics and subtropics (0° – 40°N) (Figure 6). It shows that DII in El Niño years are generally higher than in normal years ($\geq 69\%$). Specifically, the DII during El Niño years surpasses that of normal years by more than 3.6 times in top 10% watersheds (Figure 6 inset). The DII increment (ΔDII) was indicated by the difference in mean DII between El Niño years and normal years. In the regions of South Asia and East Asia, approximately 72% of watersheds exhibit a ΔDII ranging from 150% to 250%, while 14% of watersheds exceed 250%. However, in North America, 40% of watersheds have a ΔDII within 150%–250% range, and 35% of watersheds are greater than 250%.

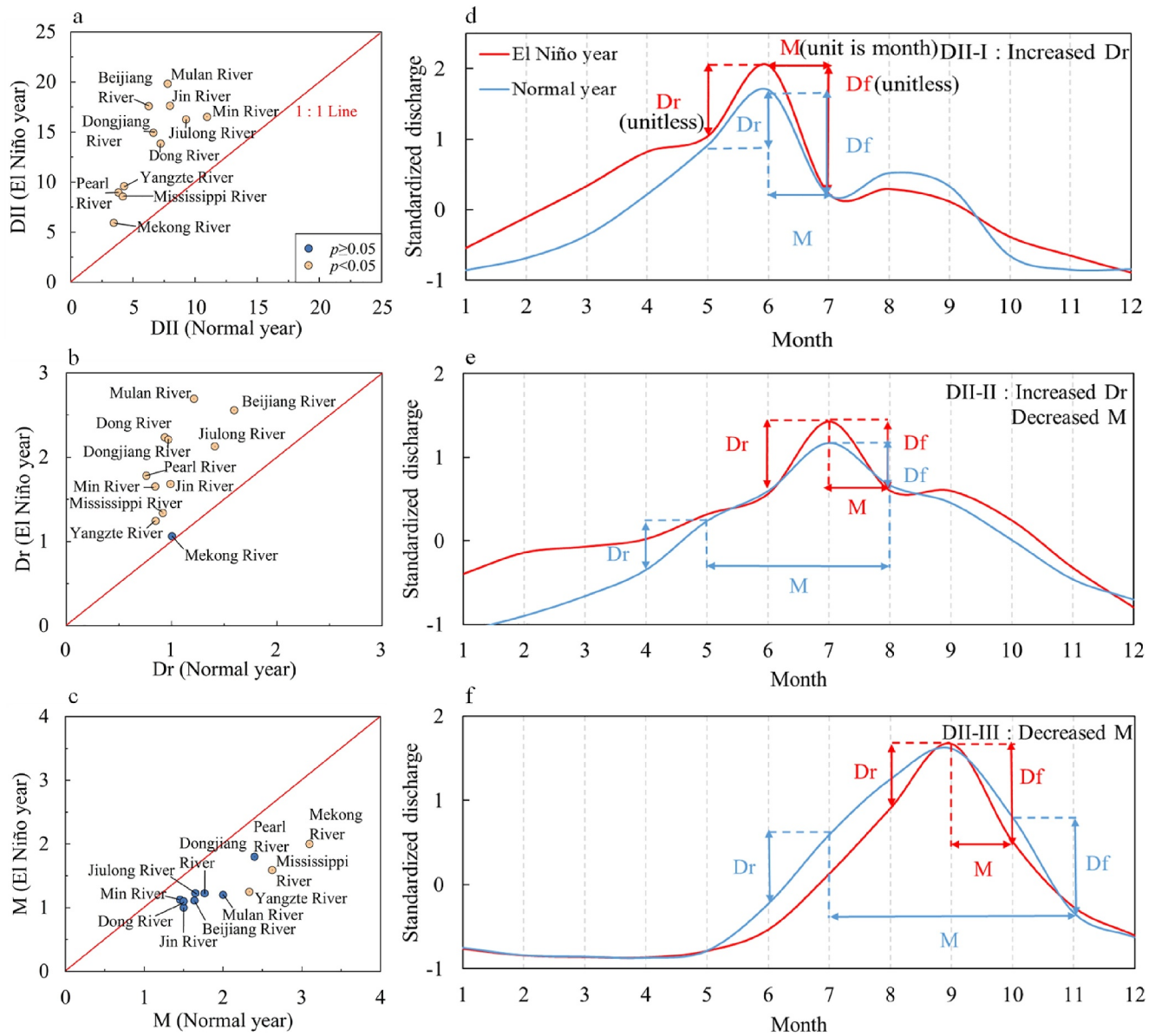


Figure 4. Variations of characterized river discharge instability indexes (a, b, c) and variations of seasonal river discharge distribution patterns in three categories (d, e, f) from El Niño years to normal years. The monthly standardized discharge was processed in El Niño years and normal years. Dr is the maximum rise of monthly standardized discharge between two adjacent months; Df is the maximum fall of monthly standardized discharge between two adjacent months; M is the timespan of months with the maximum rise and the maximum fall of river discharge; $p < 0.05$ indicates the significant difference between El Niño years and normal years based on the Mann-Whitney test. Standardized discharge in d, e, and f was the multi-year average of standardized discharge in El Niño years (red line) and normal years (blue line).

3.4. The Discharge Instability Index Under Future Climate Scenarios

The DII model of El Niño year (DII_E) was performed with SSP2-4.5 and SSP5-8.5 scenarios to predict the future trend of DII across the 284 watersheds around the Pacific Ocean in response to future climate warming. The δDII (the relative deviation (%) of future warming scenarios from current El Niño years) of the 284 watersheds ranged from 0.11% to 9.21% under the SSP2-4.5 scenario, and from 0.53% to 9.46% under the SSP5-8.5 scenario (Figure S6 in Supporting Information S1). The watersheds with high precipitation anomaly ($Pa > 5\%$) have a major increase in δDII compared to the medium Pa and low Pa watersheds (Figure 7 inset). The percentage difference of δDII between two scenarios ($\delta DII_{8.5-4.5}$) show that the δDII of SSP5-8.5 scenario were relatively greater than that of SSP2-4.5 scenario (Figure 7).

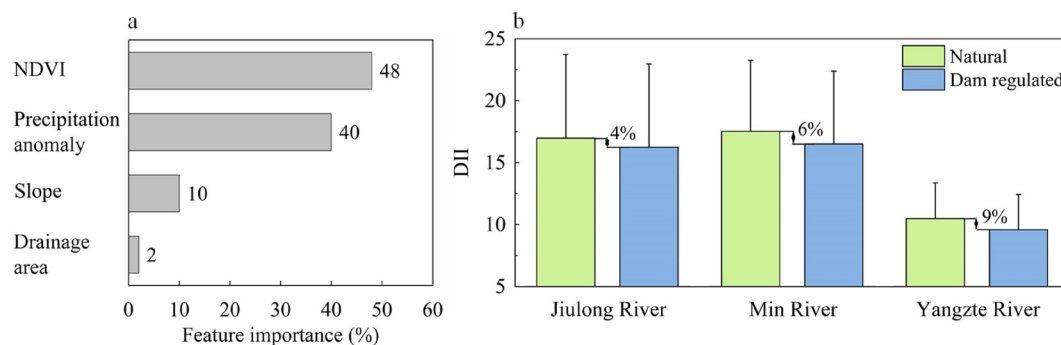


Figure 5. Feature importance of watershed characteristics to mean DII in eleven rivers by XGBoost model (a) and natural DII versus dam regulated DII (b) in El Niño years. Error bars in b are the range of variation in multi-year DII values. The number in b are the percentage difference in dam-regulated DII compared to natural DII.

4. Discussion

Our results suggest that ENSO-induced abnormal precipitation largely determine the seasonal discharge fluctuation patterns, from normal years to El Niño years (Figure 4). The DII-I (increased D_r) watersheds are mainly located in southern China like Pearl River under subtropical monsoon climate. The shift of the subtropical high-pressure system caused by El Niño triggers enhanced water vapor transportation (C-mode) from the equatorial region to southern China (Zhang et al., 2016), resulting in intensified precipitation anomaly during the rainy season and the formation of the DII-I pattern. Therefore, the DII-II (increased D_r and decreased M) watersheds are mainly situated in the mid-latitude region like Yangtze River and Mississippi River. This pattern arises from a delay in spring precipitation but an increase in summer precipitation, caused by late convergence of water vapor induced by ENSO (Chan & Zhou, 2005; Nakamura et al., 2013; Smith & Baeck, 2015). The DII-III pattern observed in the Mekong River does not exhibit an increase in D_r but displays abnormal lagged and shortened flood seasons, likely influenced by the anomalous North Pacific monsoon (WNPM) and East Asian summer winds (Räsänen & Kummu, 2013). In summary, ENSO disrupts water cycling and precipitation and impacts seasonal hydrography in watersheds.

Characterizing seasonal river discharge instability across regions remains a substantial challenge. In this study, we constructed a DII model incorporating watershed characteristics (NDVI, slope, and drainage area), in addition to precipitation anomaly, as input parameters (Figure S4a in Supporting Information S1). Based on the simulated DII increment (ΔDII) and the percentage difference of predicted DII variation between two scenarios ($\delta DII_{8.5-4.5}$), we have selected two regions (Southwestern North America and Eastern East Asia) with higher ΔDII

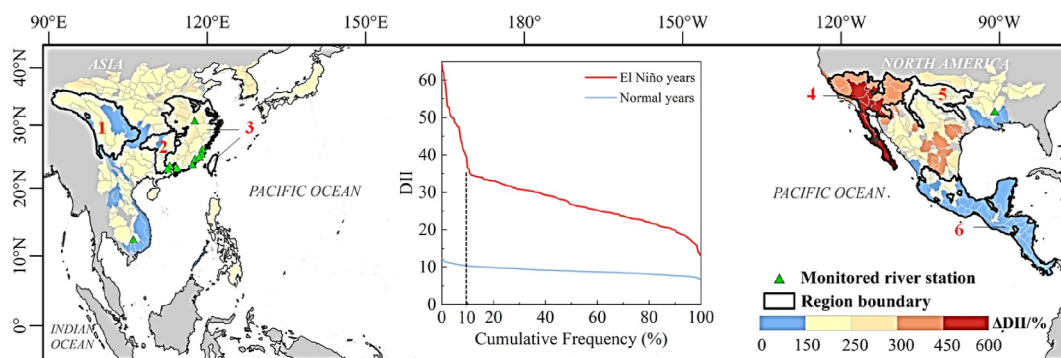


Figure 6. The distribution of modeled DII increment ($\Delta DII = (\text{the mean DII of El Niño years} - \text{the mean DII of normal years}) / \text{the mean DII of normal years} \times 100\%$). The ΔDII was calculated in 284 watersheds (the fifth level watershed in HydroBASINS data, see details in Methods), with data from 10 normal years and 7 El Niño years. Inset graph is, the ranking and proportion of watershed mean DII in El Niño years (red line) and normal years (blue line) across 284 watersheds. The black boundary shows six specific regions (1. Western East Asia; 2. Central East Asia; 3. Eastern East Asia; 4. Southwestern North America; 5. South-central North America; 6. Southern North America; detail in Table S3 in Supporting Information S1).

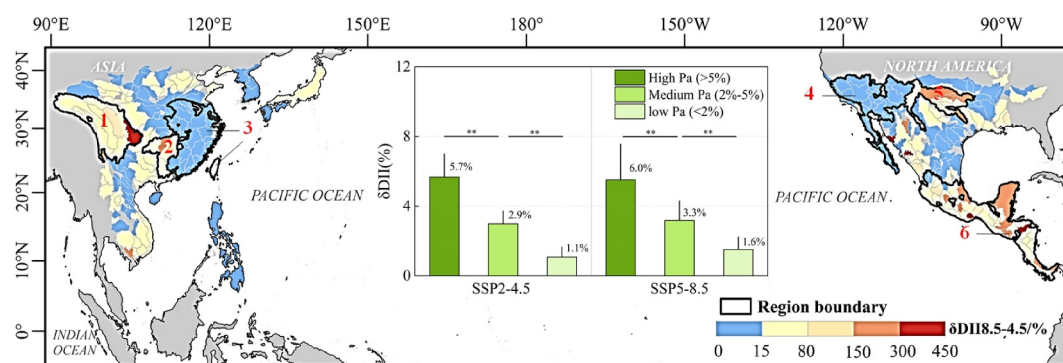


Figure 7. The distribution of percentage difference of δ DII between two scenarios (δ DII8.5–4.5) across 284 watersheds. δ DII = (the mean DII of SSP2-4.5 or SSP5-8.5 scenario—the mean DII of El Niño years)/the mean DII of El Niño years $\times 100\%$. δ DII8.5–4.5 = (the δ DII of SSP5-8.5 scenario—the δ DII of SSP2-4.5 scenario)/the δ DII of SSP2-4.5 scenario $\times 100\%$. The black boundary shows six specific regions (1. Western East Asia; 2. Central East Asia; 3. Eastern East Asia; 4. Southwestern North America; 5. South-central North America; 6. Southern North America; detail in Table S3 in Supporting Information S1). Inset graph is, the predicted DII variation (δ DII) of different precipitation anomaly (Pa) level watersheds under two warming scenarios across 284 watersheds. ** represents $p < 0.01$, indicating the significant difference in δ DII between the two types of precipitation anomalies (Pa) based on the Mann-Whitney test.

(>250%) and four regions (Western East Asia, Central East Asia, South-central North America, and Southern North America) with higher δ DII8.5–4.5 (>150%) in 284 watersheds for further discussion. The modeled DII in 284 watersheds around the Pacific Ocean between the El Niño and normal years reveal that watersheds with large DII increment (Δ DII > 300%) are primarily located in southwestern North America (Figure 6). This regional difference is related to the impact of terrain on the advection of ocean water vapor. In southwestern North America, the presence of vast plateaus and towering mountains like the West Madre lifts warm and moist air to produce convective precipitation (Boos & Pascale, 2021). The ENSO-impacted Pacific water vapor was convergence on the windward side of the mountains, resulting in abnormally heavy precipitation in the southwestern North America (Table S3 in Supporting Information S1). The higher Δ DII watersheds are mainly distributed on the windward side of the mountains in southwestern North America (including the Baja California Peninsula, the Colorado Plateau, and the Mexican Plateau). The upstream of these watersheds is mountainous, with lower NDVI (Table S3 in Supporting Information S1), indicating strong runoff production capacity. Additionally, high precipitation variation in these watersheds due to the combined influence of ENSO, the Pacific-North American pattern (PNA), and the Madden-Julian oscillation (MJO) (Grise et al., 2013). Along the Pacific coast of southern North America (the Mexican Plateau), the mountains obstruct the eastward transport of air masses (Boos & Pascale, 2021), resulting in little differences in precipitation between the El Niño year and normal year (Table S3 in Supporting Information S1). Unlike North America, the topography of East Asia is low in the east and high in the west, and the ENSO-impacted Pacific Ocean moisture spreads across the eastern of East Asia, leading to an increase in rainfall. The watersheds in the eastern plains of East Asia have a higher NDVI, and less variations in precipitation which are influenced by the weakening effect of ENSO on the precipitation due to the North Atlantic Oscillation (NAO) and Indian Ocean Dipole (IOD) (Xiao et al., 2015), corresponding to a lower Δ DII compared to southwestern North America (Table S3 in Supporting Information S1). The watersheds in western East Asia (Qinghai-Tibet Plateau) have the lowest Δ DII, as this region is less influenced by the Pacific Ocean (Tian et al., 2001).

The increased precipitation anomaly and decreased land vegetation jointly enhanced the seasonal river discharge instability but such effect strength might vary across watersheds. Since the 1980s, there has been a significant increase in global vegetation coverage, particularly in the Northern Hemisphere, referred to as “global greening” (Piao et al., 2019). However, vegetation greening and NDVI would decrease under future warming (Lian et al., 2023). Meanwhile, global warming likely produces more extreme precipitation events (i.e., Pa increase) (Trenberth, 2011). Our results suggest that increased precipitation anomaly and decreased vegetation under future warming scenarios will intensify the instability (δ DII increase 0.11%–9.46%) during El Niño years, especially in the high Pa watersheds (Figure 7 inset). The percentage difference of δ DII between two scenarios (δ DII8.5–4.5) show that a higher δ DII8.5–4.5 ($\geq 80\%$) watersheds are mainly located in southern North America (the Mexican

Plateau), western East Asia (Qinghai-Tibet Plateau), south-central North America (the Great Plains of the United States), and central East Asia (southern Sichuan Basin and eastern Yunnan-Guizhou Plateau) (Figure 7). These watersheds are located on the leeward slope of the mountain with higher NDVI (Table S3 in Supporting Information S1) (Ruiz-Barradas & Nigam, 2010; Zhang et al., 2021), and a drastic decrease in NDVI under future climate warming will produce more unstable discharge.

The enhanced river discharge instability undoubtedly poses pressure on water resource allocation. Our research implies that El Niño increases seasonal river discharge instability, leading to seasonal water shortages (Wada et al., 2011). In DII-I watersheds, there is a significant rise in floods, rendering a larger volume of floodwater unusable as a resource. In DII-II watersheds, there is an increase in floods with a shorter duration (e.g., M). This not only increases the flood control pressure during the flood season but also poses challenges to water allocation during the longer dry season. Compared to normal years, the dry season in El Niño years is prolonged by 0.1–1.1 months, while the average low flow is reduced by 0.08%–1.1% and the minimum low flow is diminished by 4.8%–7.3% (Table S4, see Text S3 in Supporting Information S1 for low flow identification). In DII-III watersheds, the dry season in El Niño years extends by 0.8 months compared to normal years, and both the average and minimum low flows decrease by 2.3% and 4.2%, respectively. The scarcity of water resources exacerbates competition among various water usage such as agricultural production, potable water supply, and the ecological flows. In addition, the anomalous fluctuations in seasonal river discharge and the rising occurrence of extreme events further contribute to the mounting water stress caused by population growth (Oki & Kanae, 2006).

The ENSO-impacted watersheds require the implementation of specific regulatory measures as an adaptation strategy to future climate change. For the DII-I watersheds, it is necessary to utilize the functionality of dams in regulating high flow pulses (Chaudhari & Pokhrel, 2022). For the DII-II and DII-III pattern watersheds, further optimize the operation of the reservoir and improve its dispatching capacity during dry season and storage capacity during flood season. Meanwhile, coordinated regulation of cascade reservoir dams within the entire watershed (across watersheds in some cases) is necessary to improve the seasonal allocation of water resources. However, overuse of dams can lead to river fragmentation and eutrophication (Belletti et al., 2020; Xiang et al., 2021). The conflict between promoting renewable hydropower and restoring aquatic ecosystems becomes increasingly apparent (Carolli et al., 2023; Consuegra et al., 2021). Therefore, it is crucial to prioritize the restoration of degraded lands or afforestation to enhance water-holding capacity, especially in watersheds with high precipitation anomalies. To sustain the current DII amidst future warming, a 9% rise in NDVI in southwestern North America and a 2%–4% increase in other regions is essential (see Text S4 in Supporting Information S1). These measures aim to reduce seasonal river discharge instability and alleviate water resource allocation pressure arising from ENSO event.

The efficacy of water resources management measures in response to ENSO is heavily contingent upon the precision of ENSO forecasts. However, current forecasting models struggle to offer reliable predictions for lead times extending beyond the 6–10 months mark (Ham et al., 2019). This limitation introduces significant challenges for seasonal ENSO management (Cai et al., 2018), which underscores the increased variability and unpredictability of Eastern Pacific El Niño events under the influence of greenhouse warming. To effectively manage water resources amidst the unpredictability of ENSO, we recommend a dual-strategy approach that combines short term action with long-term planning. In the short term, water managers should employ advanced real-time monitoring and predictive model system to guide responsive dam operations and water flow allocation. For the long term, we advocate for the development and implementation of comprehensive strategies that enhance the resilience and sustainability of water systems. A key component of these strategies is watershed afforestation. By restoring and preserving natural vegetation, we can reduce soil erosion, increase groundwater recharge, and create a more robust buffer against extreme weather events. By integrating these short-term adaptive measures with long-term resilience-building strategies, water managers can more effectively manage the uncertainties associated with ENSO and ensure the sustainable stewardship of water resources. This comprehensive approach, underpinned by ongoing advancements in climate science and technology, is essential for adapting to the complexities of a changing climate.

Furthermore, it is essential to recognize that a variety of climate change modes, beyond ENSO, significantly influence water resource dynamics. The Pacific Decadal Oscillation (PDO), for instance, has been shown to amplify the variability of water flows in southern East Asia (Delgado et al., 2012; Zhang et al., 2015). Additionally, the PDO has been linked to the creation of abnormally wet conditions in southwestern North America

and Mexico (Dong & Dai, 2015; Villarini et al., 2014), which in turn can precipitate more frequent large-scale flooding events (Whited et al., 2007). Similarly, the North Atlantic Oscillation (NAO) has been identified as a key factor that elevates the probability of extreme rainfall events (Wang et al., 2014; Whan & Zwiers, 2017). This climatic pattern also plays a significant role in the severity of flood events in eastern North America. On the other hand, the Atlantic Multi-decadal Oscillation (AMO) has been found to exhibit a substantial negative correlation with flood events across North America (Hodgkins et al., 2017; Valdés-Manzanilla, 2016). This suggests that periods of high AMO activity may be associated with a reduced risk of flooding.

In light of these findings, it is imperative for water resource managers to adopt a holistic approach when formulating strategies to address climate change. This includes considering the collective impacts of various climate modes, such as the PDO, NAO, and AMO, alongside the well-recognized influence of ENSO. By integrating a comprehensive understanding of these climate phenomena, managers can develop more effective and adaptive water management plans that are resilient to the multifaceted challenges posed by climate change.

5. Uncertainty and Limitation

In the current El Niño year and future warming scenarios, the DII variations (Δ DII and δ DII_{8.5–4.5}) using GPCC, show a decrease of 12%–38% compared to the DII variations using CRU in the 284 watersheds (Figure S7 in Supporting Information S1). The Δ DII calculated using CRU is 1–3 times higher than that using GPCC in over 70% of the watersheds (Figure S7a in Supporting Information S1). In 80% of the 284 watersheds, the comparison of δ DII_{8.5–4.5} calculated using CRU and GPCC (δ DII_{8.5–4.5}(CRU)/ δ DII_{8.5–4.5}(GPCC)) falls between 0 and 2 (Figure S7b in Supporting Information S1). These differences may be attributed to the fact that the GPCC database includes around 3–4 times as many precipitation stations as CRU. The difference in DII variations using MODIS compared to GIMMS3g is –11%–37%. The Δ DII calculated using GIMMS3g is higher than that calculated using MODIS (approximately 1–3 times) in 80% of the 284 watersheds (Figure S8a in Supporting Information S1), and the δ DII_{8.5–4.5} calculated using GIMMS3g is lower than that calculated using MODIS (approximately 0–1 times) in 99% of the 284 watersheds (Figure S8b in Supporting Information S1). The results from different data sets all demonstrate that intensifying the instability of seasonal river discharge, and future warming will enhance the instability, which enhances the robustness of the findings from this study.

In the development of the DII model, data from eleven selected watersheds were utilized, with the limited sample size dictating the application of a stepwise regression approach. The 95% confidence interval of the DII_E and DII_N model ranges from –12% to 14%. The biases related to the model in Δ DII range from –3% to –16% across the 284 watersheds, while the δ DII_{8.5–4.5} shows no bias related to the DII_E model as it is a relative percentage difference. Currently, the chosen watersheds are confined to Asia and North America. However, the ENSO event exerts a distinct influence on the seasonal river flows in African, European, and Oceania basins, varying from those in Asia and North America (Ward et al., 2014). To advance this field, future studies should prioritize data integrity and augment the data set with a greater number of watershed examples, thereby facilitating the employment of more predictive data-driven models (such as machine learning models), and offering more precise data support for seasonal ENSO management on a global scale. Future warming scenarios are predicted to amplify the instability of river discharge. The future ENSO-driven precipitation anomaly rate (15% increase) used to calculate precipitation anomalies under future warming scenarios is based on CMIP5 models (one of the climate models). However, such climate models exhibit stubborn climate biases in the eastern equatorial Pacific, which may affect their representation of feedback and ENSO complexity, as well as the fidelity of operational ENSO forecasts (Timmermann et al., 2018). This may lead to an underestimation of ENSO precipitation variability under future climate warming scenarios (Power & Delage, 2018). It is importance to prioritize the restoration of degraded lands or afforestation to enhance water-holding capacity to cope with enhanced ENSO precipitation variability under future climate change. In addition, the variability of ENSO sea surface temperature will increase in the future (Cai et al., 2018), and future water crisis could be more severe than anticipated (Zhang et al., 2023). The impact of ENSO events on the instability of river flow under future climate warming requires a next-generation climate model that can better simulate ENSO for accurate prediction.

6. Conclusion

We investigated the impact of ENSO on seasonal fluctuations in river discharge across watersheds in the regions of South Asia, East Asia, and North America surrounding the Pacific Ocean. Our results confirm that El Niño

event led to more unstable discharge in the 284 analyzed watersheds of this region. The main conclusions are highlighted below:

1. We identified the ENSO-impact seasonal distribution patterns via key hydrograph features. ENSO intensifies Dr in eleven monitored watersheds representing South Asia, East Asia, and North America regions, and decreases M in larger rivers like the Yangtze River.
2. We quantified the uneven seasonal distribution of river discharge through a new index called discharge instability index (DII). ENSO intensifies the instability of seasonal river discharge during El Niño years compared to normal years. The higher DII was observed in southwestern North American watersheds due to higher precipitation anomaly. The increment in discharge instability will vary across 284 watersheds, mainly influenced by vegetation and abnormal precipitation.
3. Future warming scenarios are projected to amplify the instability of river discharge. The watersheds with high precipitation anomaly ($P_a > 5\%$) has have a major increase in DII across 284 watersheds.

This research contributes to a better understanding of the complex interactions between ENSO, river discharge, and water resources. It emphasizes the importance of addressing these challenges in order to ensure the reliability and sustainability of water resource allocation. We champion the implementation of customized regulatory strategies that consider the unique characteristics of individual watersheds. Our approach integrates immediate interventions, such as dam management, with comprehensive long-term initiatives like afforestation. This dual strategy aims to alleviate the adverse effects of climate change on the distribution and management of water resources.

Conflict of Interest

The authors declare no conflicts of interest relevant to this study.

Data Availability Statement

For the Niño Index (ONI) data was collected from Golden Gate Weather Services (<https://ggweather.com/enso/oni.htm>). For the watersheds boundary was collected from HydroBASINS data (<https://hydrosheds.org/page/overview>). For the discharge data from stations (i.e., Shijiao, Boluo, and Gaoyao on Pearl River, Kratie on Mekong River, Vicksburg on Mississippi River) were obtained from the Global Runoff Data Centre (<https://www.bafg.de>), and other stations (Laixi on Mulan River, Zhao'an on Dong River, Shilong on Jin River, Punan on Jiulong River, Zhuqi on the Min River, Datong on the Yangtze River) were obtained from the Fujian Water Resources Survey Center (measured data, available on request). For the daily meteorological data were obtained from China Meteorological Data Service Centre (<https://www.cma.gov.cn/>) and Climatic Research Unit gridded Time Series (<https://crudata.uea.ac.uk/cru/data/hrg/>). For Digital Elevation Model (DEM) on a 30 by 30 m grid was obtained from the geospatial data cloud platform (<https://www.gscloud.cn/>). For the GIMMS 3g Normalized Difference Vegetation Index (NDVI) with a spatial resolution of 0.0833° from ECOCAST (<http://ecocast.arc.nasa.gov>).

References

- Amarasekera, K. N., Lee, R. F., Williams, E. R., & Eltahir, E. A. B. (1997). ENSO and the natural variability in the flow of tropical rivers. *Journal of Hydrology*, 200(1–4), 24–39. [https://doi.org/10.1016/s0022-1694\(96\)03340-9](https://doi.org/10.1016/s0022-1694(96)03340-9)
- Becker, A., Finger, P., Meyer-Christoffer, A., Rudolf, B., Schamm, K., Schneider, U., & Ziese, M. (2013). A description of the global land-surface precipitation data products of the global Precipitation Climatology Centre with sample applications including centennial (trend) analysis from 1901–present. *Earth System Science Data*, 5(1), 71–99. <https://doi.org/10.5194/essd-5-71-2013>
- Belletti, B., Garcia de Leaniz, C., Jones, J., Bizzi, S., Börger, L., Segura, G., et al. (2020). More than one million barriers fragment Europe's rivers. *Nature*, 588(7838), 436–441. <https://doi.org/10.1038/s41586-020-3005-2>
- Boos, W. R., & Pascale, S. (2021). Mechanical forcing of the North American monsoon by orography. *Nature*, 599(7886), 611–615. <https://doi.org/10.1038/s41586-021-03978-2>
- Cai, W., Wang, G., Dewitte, B., Wu, L., Santoso, A., Takahashi, K., et al. (2018). Increased variability of Eastern Pacific El Niño under greenhouse warming. *Nature*, 564(7735), 201–206. <https://doi.org/10.1038/s41586-018-0776-9>
- Cai, W. J., Wang, G., Santoso, A., McPhaden, M. J., Wu, L., Jin, F. F., et al. (2015). Increased frequency of extreme La Nina events under greenhouse warming. *Nature Climate Change*, 5(2), 132–137. <https://doi.org/10.1038/nclimate2492>
- Cai, W. J., Wang, G. J., Santoso, A., Lin, X. P., & Wu, L. X. (2017). Definition of extreme El Niño and its impact on projected increase in extreme El Niño frequency. *Geophysical Research Letters*, 44(21), 11184–11190. <https://doi.org/10.1002/2017gl075635>
- Carolli, M., de Leaniz, C. G., Jones, J., Belletti, B., Hudek, H., Pusch, M., et al. (2023). Impacts of existing and planned hydropower dams on river fragmentation in the Balkan region. *Science of the Total Environment*, 871, 161940. <https://doi.org/10.1016/j.scitotenv.2023.161940>

Acknowledgments

This research was supported by the National Natural Science Foundation of China (Nos. 41376082, 42325702). We thank the Hydrology and Water Resources Survey Center of Zhangzhou, Province Fujian for providing flow data. China Meteorological Data Service Centre, National Earth System Science Data Center, Geospatial Data Cloud, Global Runoff Data Centre, and University of East Anglia for making some data publicly available.

- Chan, J. C. L., & Zhou, W. (2005). PDO, ENSO and the early summer monsoon rainfall over south China. *Geophysical Research Letters*, 32(8), L08810. <https://doi.org/10.1029/2004gl020215>
- Chaudhari, S., & Pokhrel, Y. (2022). Alteration of river flow and flood dynamics by existing and planned hydropower dams in the amazon river basin. *Water Resources Research*, 58(5), e2021WR030555. <https://doi.org/10.1029/2021wr030555>
- Chen, Z. F., Wang, W. G., Woods, R. A., & Shao, Q. X. (2021). Hydrological effects of change in vegetation components across global catchments. *Journal of Hydrology*, 595, 125775. <https://doi.org/10.1016/j.jhydrol.2020.125775>
- Consuegra, S., O'Rourke, R., Rodríguez-Barreto, D., Fernández, S., Jones, J., & García de Leaniz, C. (2021). Impacts of large and small barriers on fish assemblage composition assessed using environmental DNA metabarcoding. *Science of the Total Environment*, 790, 148054. <https://doi.org/10.1016/j.scitotenv.2021.148054>
- Delgado, J. M., Merz, B., & Apel, H. (2012). A climate-flood link for the lower Mekong River. *Hydrology and Earth System Sciences*, 16(5), 1533–1541. <https://doi.org/10.5194/hess-16-1533-2012>
- Dong, B., & Dai, A. G. (2015). The influence of the Interdecadal Pacific Oscillation on temperature and precipitation over the globe. *Climate Dynamics*, 45(9–10), 2667–2681. <https://doi.org/10.1007/s00382-015-2500-x>
- Eliasson, J. (2015). The rising pressure of global water shortages. *Nature*, 517(7532), 6. <https://doi.org/10.1038/517006a>
- Emerton, R., Cloke, H. L., Stephens, E. M., Zsoter, E., Woolnough, S. J., & Pappenberger, F. (2017). Complex picture for likelihood of ENSO-driven flood hazard. *Nature Communications*, 8(1), 14796. <https://doi.org/10.1038/ncomms14796>
- Good, P., Chadwick, R., Holloway, C. E., Kennedy, J., Lowe, J. A., Roehrig, R., & Rushey, S. S. (2021). High sensitivity of tropical precipitation to local sea surface temperature. *Nature*, 589(7842), 408–414. <https://doi.org/10.1038/s41586-020-2887-3>
- Grise, K. M., Son, S. W., & Gyakum, J. R. (2013). Intraseasonal and interannual variability in North American storm tracks and its relationship to equatorial pacific variability. *Monthly Weather Review*, 141(10), 3610–3625. <https://doi.org/10.1175/MWR-D-12-00322.1>
- Ham, Y. G., Kim, J. H., & Luo, J. J. (2019). Deep learning for multi-year ENSO forecasts. *Nature*, 573(7775), 568–572. <https://doi.org/10.1038/s41586-019-1559-7>
- Harris, I., Osborn, T. J., Jones, P., & Lister, D. (2020). Version 4 of the CRU TS monthly high-resolution gridded multivariate climate dataset. *Scientific Data*, 7(1), 109. <https://doi.org/10.1038/s41597-020-0453-3>
- Hodgkins, G. A., Whitfield, P. H., Burn, D. H., Hannaford, J., Renard, B., Stahl, K., et al. (2017). Climate-driven variability in the occurrence of major floods across North America and Europe. *Journal of Hydrology*, 552, 704–717. <https://doi.org/10.1016/j.jhydrol.2017.07.027>
- Kawamura, K., Akiyama, T., Yokota, H.-O., Tsutsumi, M., Yasuda, T., Watanabe, O., & Wang, S. (2005). Comparing MODIS vegetation indices with AVHRR NDVI for monitoring the forage quantity and quality in inner Mongolia grassland, China. *Grassland Science*, 51(1), 33–40. <https://doi.org/10.1111/j.1744-697X.2005.00006.x>
- Krasovskaia, I. (1997). Entropy-based grouping of river flow regimes. *Journal of Hydrology*, 202(1–4), 173–191. [https://doi.org/10.1016/s0022-1694\(97\)00065-6](https://doi.org/10.1016/s0022-1694(97)00065-6)
- Larsen, T. A., Hoffmann, S., Lüthi, C., Truffer, B., & Maurer, M. (2016). Emerging solutions to the water challenges of an urbanizing world. *Science*, 352(6288), 928–933. <https://doi.org/10.1126/science.aad8641>
- Lehner, B., & Grill, G. (2013). Global river hydrography and network routing: Baseline data and new approaches to study the world's large river systems. *Hydrological Processes*, 27(15), 2171–2186. <https://doi.org/10.1002/hyp.9740>
- Lian, X., Jiao, L., Hu, Y., & Liu, Z. (2023). Future climate imposes pressure on vulnerable ecological regions in China. *Science of the Total Environment*, 858, 159995. <https://doi.org/10.1016/j.scitotenv.2022.159995>
- Liu, J., & Yang, W. (2012). Water sustainability for China and beyond. *Science*, 337(6095), 649–650. <https://doi.org/10.1126/science.1219471>
- Ma, F., Ye, A. Z., You, J. J., & Duan, Q. Y. (2018). 2015–16 floods and droughts in China, and its response to the strong El Niño. *Science of the Total Environment*, 627, 1473–1484. <https://doi.org/10.1016/j.scitotenv.2018.01.280>
- McPhaden, M. J., Zebiak, S. E., & Glantz, M. H. (2006). ENSO as an integrating concept in earth science. *Science*, 314(5806), 1740–1745. <https://doi.org/10.1126/science.1132588>
- Nakamura, J., Lall, U., Kushnir, Y., Robertson, A. W., & Seager, R. (2013). Dynamical structure of extreme floods in the U.S. Midwest and the United Kingdom. *Journal of Hydrometeorology*, 14(2), 485–504. <https://doi.org/10.1175/jhm-d-12-059.1>
- Oki, T., & Kanae, S. (2006). Global hydrological cycles and world water resources. *Science*, 313(5790), 1068–1072. <https://doi.org/10.1126/science.1128845>
- Ouyang, R., Liu, W., Fu, G., Liu, C., Hu, L., & Wang, H. (2014). Linkages between ENSO/PDO signals and precipitation, streamflow in China during the last 100 years. *Hydrology and Earth System Sciences*, 18(9), 3651–3661. <https://doi.org/10.5194/hess-18-3651-2014>
- Piao, S., Wang, X., Park, T., Chen, C., Lian, X., He, Y., et al. (2019). Characteristics, drivers and feedbacks of global greening. *Nature Reviews Earth & Environment*, 1(1), 14–27. <https://doi.org/10.1038/s43017-019-0001-x>
- Power, S. B., & Delage, F. P. D. (2018). El Niño Southern Oscillation and associated climatic conditions around the world during the latter half of the twenty-first century. *Journal of Climate*, 31(15), 6189–6207. <https://doi.org/10.1175/jcli-d-18-0138.1>
- Räsänen, T. A., & Kumm, M. (2013). Spatiotemporal influences of ENSO on precipitation and flood pulse in the Mekong river basin. *Journal of Hydrology*, 476, 154–168. <https://doi.org/10.1016/j.jhydrol.2012.10.028>
- Rice, J. S., & Emanuel, R. E. (2017). How are streamflow responses to the El Niño Southern Oscillation affected by watershed characteristics? *Water Resources Research*, 53(5), 4393–4406. <https://doi.org/10.1002/2016wr020097>
- Ruiz-Barradas, A., & Nigam, S. (2010). Great plains precipitation and its SST links in twentieth-century climate simulations, and twenty-first- and twenty-second-century climate projections. *Journal of Climate*, 23(23), 6409–6429. <https://doi.org/10.1175/2010jcli3173.1>
- Shrestha, A., & Kostaschuk, R. (2005). El Niño/Southern Oscillation (ENSO)-related variability in mean-monthly streamflow in Nepal. *Journal of Hydrology*, 308(1–4), 33–49. <https://doi.org/10.1016/j.jhydrol.2004.10.020>
- Siam, M. S., & Eltahir, E. A. B. (2017). Climate change enhances interannual variability of the Nile river flow. *Nature Climate Change*, 7(5), 350–354. <https://doi.org/10.1038/nclimate3273>
- Siegert, F., Ruecker, G., Hinrichs, A., & Hoffmann, A. A. (2001). Increased damage from fires in logged forests during droughts caused by El Niño. *Nature*, 414(6862), 437–440. <https://doi.org/10.1038/35106547>
- Singh, J., Ashfaq, M., Skinner, C. B., Anderson, W. B., Mishra, V., & Singh, D. (2022). Enhanced risk of concurrent regional droughts with increased ENSO variability and warming. *Nature Climate Change*, 12(4), 408. <https://doi.org/10.1038/s41558-022-01340-6>
- Smith, J. A., & Baeck, M. L. (2015). Prophetic vision, vivid imagination: The 1927 Mississippi river flood. *Water Resources Research*, 51(12), 9964–9994. <https://doi.org/10.1002/2015wr017927>
- Su, L., Miao, C. Y., Kong, D. X., Duan, Q. Y., Lei, X. H., Hou, Q. Q., & Li, H. (2018). Long-term trends in global river flow and the causal relationships between river flow and ocean signals. *Journal of Hydrology*, 563, 818–833. <https://doi.org/10.1016/j.jhydrol.2018.06.058>
- Sun, X., Renard, B., Thyer, M., Westra, S., & Lang, M. (2015). A global analysis of the asymmetric effect of ENSO on extreme precipitation. *Journal of Hydrology*, 530, 51–65. <https://doi.org/10.1016/j.jhydrol.2015.09.016>

- Tian, L., Masson-Delmotte, V., Stievenard, M., Yao, T., & Jouzel, J. (2001). Tibetan plateau summer monsoon northward extent revealed by measurements of water stable isotopes. *Journal of Geophysical Research*, *106*(D22), 28081–28088. <https://doi.org/10.1029/2001jd900186>
- Timmermann, A., An, S. I., Kug, J. S., Jin, F. F., Cai, W., Capotondi, A., et al. (2018). El Niño–Southern oscillation complexity. *Nature*, *559*(7715), 535–545. <https://doi.org/10.1038/s41586-018-0252-6>
- Trenberth, K. E. (2011). Changes in precipitation with climate change. *Climate Research*, *47*(1–2), 123–138. <https://doi.org/10.3354/cr00953>
- Valdés-Manzanilla, A. (2016). Historical floods in Tabasco and Chiapas during sixteenth–twentieth centuries. *Natural Hazards*, *80*(3), 1563–1577. <https://doi.org/10.1007/s11069-015-2039-5>
- Villarini, G., Goska, R., Smith, J. A., & Vecchi, G. A. (2014). North Atlantic tropical cyclones and U.S. flooding. *Bulletin of the American Meteorological Society*, *95*(9), 1381–1388. <https://doi.org/10.1175/bams-d-13-00060.1>
- Vörösmarty, C. J., McIntyre, P. B., Gessner, M. O., Dudgeon, D., Prusevich, A., Green, P., et al. (2010). Global threats to human water security and river biodiversity. *Nature*, *467*(7315), 555–561. <https://doi.org/10.1038/nature09440>
- Wada, Y., van Beek, L. P. H., Viviroli, D., Dürr, H. H., Weingartner, R., & Bierkens, M. F. P. (2011). Global monthly water stress: 2. Water demand and severity of water stress. *Water Resources Research*, *47*(7), W07518. <https://doi.org/10.1029/2010wr009792>
- Wang, P. X., Wang, B., Cheng, H., Fasullo, J., Guo, Z., Kiefer, T., & Liu, Z. (2017). The global monsoon across time scales: Mechanisms and outstanding issues. *Earth-Science Reviews*, *174*, 84–121. <https://doi.org/10.1016/j.earscirev.2017.07.006>
- Wang, S., Zhou, Y., You, X. X., Wang, B., & Du, L. N. (2023). Quantification of the antagonistic and synergistic effects of Pb²⁺, Cu²⁺, and Zn²⁺ bioaccumulation by living bacillus subtilis biomass using XGBoost and SHAP. *Journal of Hazardous Materials*, *446*, 130635. <https://doi.org/10.1016/j.jhazmat.2022.130635>
- Wang, S. Y., Hakala, K., Gillies, R. R., & Capehart, W. J. (2014). The Pacific Quasi-Decadal Oscillation (QDO): An important precursor toward anticipating major flood events in the Missouri river basin? *Geophysical Research Letters*, *41*(3), 991–997. <https://doi.org/10.1002/2013gl059042>
- Ward, P. J., Eisner, S., Florke, M., Dettinger, M. D., & Kummu, M. (2014). Annual flood sensitivities to El Niño–Southern Oscillation at the global scale. *Hydrology and Earth System Sciences*, *18*(1), 47–66. <https://doi.org/10.5194/hess-18-47-2014>
- Whan, K., & Zwiers, F. (2017). The impact of ENSO and the NAO on extreme winter precipitation in North America in observations and regional climate models. *Climate Dynamics*, *48*(5–6), 1401–1411. <https://doi.org/10.1007/s00382-016-3148-x>
- Whited, D. C., Lorang, M. S., Harner, M. J., Hauer, F. R., Kimball, J. S., & Stanford, J. A. (2007). Climate, hydrologic disturbance, and succession: Drivers of floodplain pattern. *Ecology*, *88*(4), 940–953. <https://doi.org/10.1890/05-1149>
- Xiang, R., Wang, L. J., Li, H., Tian, Z. B., & Zheng, B. H. (2021). Water quality variation in tributaries of the three gorges reservoir from 2000 to 2015. *Water Research*, *195*, 116993. <https://doi.org/10.1016/j.watres.2021.116993>
- Xiao, M. Z., Zhang, Q., & Singh, V. P. (2015). Influences of ENSO, NAO, IOD and PDO on seasonal precipitation regimes in the Yangtze River basin, China. *International Journal of Climatology*, *35*(12), 3556–3567. <https://doi.org/10.1002/joc.4228>
- Zhang, Q., Gu, X. H., Singh, V. P., Xiao, M. Z., & Chen, X. H. (2015). Evaluation of flood frequency under non-stationarity resulting from climate indices and reservoir indices in the East River basin, China. *Journal of Hydrology*, *527*, 565–575. <https://doi.org/10.1016/j.jhydrol.2015.05.029>
- Zhang, Q., Xu, C. Y., Jiang, T., & Wu, Y. J. (2007). Possible influence of ENSO on annual maximum streamflow of the Yangtze river, China. *Journal of Hydrology*, *333*(2–4), 265–274. <https://doi.org/10.1016/j.jhydrol.2006.08.010>
- Zhang, S. H., Liu, B., Ren, G. Y., Zhou, T. J., Jiang, C., Li, S. F., & Su, B. H. (2021). Moisture sources and paths associated with warm-season precipitation over the Sichuan basin in southwestern China: Climatology and interannual variability. *Journal of Hydrology*, *603*, 127019. <https://doi.org/10.1016/j.jhydrol.2021.127019>
- Zhang, W. J., Li, H. Y., Stuecker, M. F., Jin, F. F., & Turner, A. G. (2016). A new understanding of El Niño's impact over east Asia: Dominance of the ENSO combination mode. *Journal of Climate*, *29*(12), 4347–4359. <https://doi.org/10.1175/jcli-d-15-0104.1>
- Zhang, Y. L., Song, C. H., Band, L. E., Sun, G., & Li, J. X. (2017). Reanalysis of global terrestrial vegetation trends from MODIS products: Browning or greening? *Remote Sensing of Environment*, *191*, 145–155. <https://doi.org/10.1016/j.rse.2016.12.018>
- Zhang, Y. Q., Zheng, H., Zhang, X., Leung, L. R., Liu, C., Zheng, C., et al. (2023). Future global streamflow declines are probably more severe than previously estimated. *Nature Water*, *1*(3), 261–271. <https://doi.org/10.1038/s44221-023-00030-7>
- Zhang, Z. Y., Liu, J. H., & Huang, J. L. (2020). Hydrologic impacts of cascade dams in a small headwater watershed under climate variability. *Journal of Hydrology*, *590*, 125426. <https://doi.org/10.1016/j.jhydrol.2020.125426>